Applied Energy 211 (2018) 431–442

Contents lists available at ScienceDirect

Applied Energy

journal homepage: www.elsevier.com/locate/apenergy

$Ca_2Fe_2O_5$: A promising oxygen carrier for CO/CH_4 conversion and almost-pure H_2 production with inherent CO_2 capture over a two-step chemical looping hydrogen generation process

Zhao Sun[a,b], Shiyi Chen[a], Jun Hu[a], Aimin Chen[c], Asif Hasan Rony[b], Christopher K. Russell[d], Wenguo Xiang[a,*], Maohong Fan[b,*], M. Darby Dyar[e], Elizabeth C. Dklute[e]

[a] Key Laboratory of Energy Thermal Conversion and Control of Ministry of Education, School of Energy and Environment, Southeast University, Nanjing 210096, China
[b] Departments of Chemical and Petroleum Engineering, University of Wyoming, Laramie, WY 82071, USA
[c] College of Chemical Engineering, Zhejiang University of Technology, Hangzhou 310023, China
[d] Department of Civil and Environmental Engineering, Stanford University, Stanford, CA 94305, USA
[e] Mount Holyoke College, Department of Earth & Environment, South Hadley, MA 01075, USA

HIGHLIGHTS

- A modified sol–gel method was used for the preparation of oxygen carriers.
- A two-step chemical looping hydrogen generation process is proposed.
- The existence of Ca shows significant effect on the Fe^{3+} reduction and Fe^0 oxidation.
- The hydrogen yields could be increased by using $Ca_2Fe_2O_5$ as oxygen carrier.

GRAPHICAL ABSTRACT

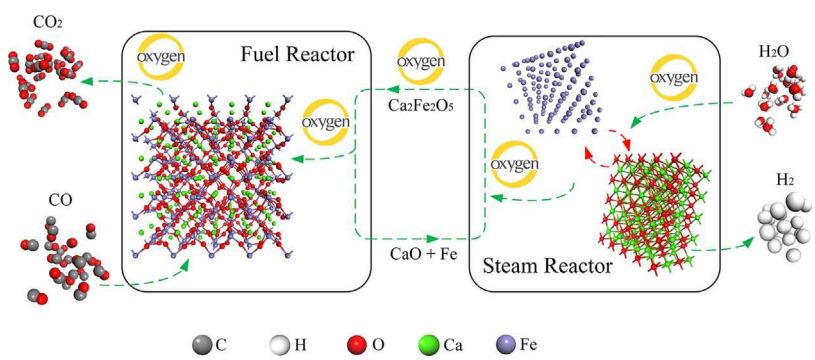

ARTICLE INFO

Keywords:
Chemical looping
Hydrogen generation
TCLHG
CO_2capture
$Ca_2Fe_2O_5$
Oxygen carrier

ABSTRACT

Chemical looping hydrogen generation (CLHG) is a promising technology for high-purity hydrogen production with inherent CO_2 separation. The selection of a high-performance oxygen carrier capable of being reduced and oxidized over multiple redox cycles against deactivation is a key issue for CLHG technology. In this work, a two-step chemical looping hydrogen generation (TCLHG) process is proposed by using a novel calcium ferrite, $Ca_2Fe_2O_5$, as an oxygen carrier which is synthesized with applied a citric acid assisted sol–gel method. The experimental results indicate that the reduced oxygen carrier achieves one-step oxidation from Fe^0 to Fe^{3+} by using steam as an oxidizing agent. Thus, higher yields of hydrogen could be generated compared with Fe_2O_3. The fresh and reacted Ca-Fe based oxygen carriers were characterized using different methods such as XRD, SEM/EDS, TEM, N_2 adsorption, H_2-TPR, XPS, and Mossbauer spectroscopy test etc. The oxygen release and storage capacity, cyclic stability, and carbon deposition characteristics of the Ca-Fe based oxygen carriers were investigated using TGA and a fixed bed reactor with multicycles of CO/CH_4 reduction and H_2O/O_2 oxidation. $Ca_2Fe_2O_5$ is proved to be a more stable formation of the calcium ferrite compounds and a promising oxygen carrier for TCLHG process which shows perfect reducibility, oxidation activity, and cyclic stability. The existence

* Corresponding authors.
E-mail address: wgxiang@seu.edu.cn (W. Xiang).

https://doi.org/10.1016/j.apenergy.2017.11.005
Received 12 August 2017; Received in revised form 15 October 2017; Accepted 1 November 2017
Available online 20 November 2017
0306-2619/

of Ca appears to perform a significant effect on the Fe^{3+} reduction and Fe^0 oxidation and the reduction from Fe^{3+} to Fe^0 was concluded to be a simple one-step reaction.

1. Introduction

Hydrogen is expected to be one of the most important energy carriers in the near future due to its increasing use in hydro-processing and hydrocracking processes and as a reduced emission fuel in combustion engines and fuel cells [1–4]. Generally, fossil fuels are used as the feedstock for hydrogen production (e.g. biomass gasification, coal gasification, and steam methane reforming). Steam-reforming of methane is currently the dominant method for large-scale H_2 production, followed by the processes of water gas shift, acid gas treatment, and pressure swing adsorption [5,6]. However, the process is complicated and the energy consumption of pressure swing adsorption is huge [7,8]. The more serious problem is a large amount of CO_2 is released into the atmosphere which aggravates the global warming. Therefore, to meet the projected demand for cheap, stable, and clean hydrogen production, an innovative hydrogen production process with a higher energy conversion efficiency, lower investment cost, and fewer environmental hazards is urgently required.

From the environmental standpoint, the chemical looping process shows the potential to capture 100% carbon from the fuels and without additional CO_2 separation steps [9,10]. Chemical looping hydrogen generation (CLHG) has been proposed as a promising technology for high-purity hydrogen production with high conversion efficiency and CO_2 separation [11,12]. The CLHG process, using iron oxide as an oxygen carrier, is generally comprised of three reactors: a fuel reactor (FR), where the carbonaceous fuel (biomass, coal, or natural gas) is oxidized to form CO_2 and H_2O; a steam reactor (SR), where the reduced oxygen carrier is oxidized by steam to produce high concentration of H_2; and an air reactor (AR), where the partially oxidized oxygen carrier is regenerated to its initial state by air [11,13,14]. The chemical reaction occurring in the CLHG process, using carbon monoxide (CO) as the fuel and ferric oxide (Fe_2O_3) as the oxygen carrier, are summarized as follows:

Fuel reactor (FR):

$$3Fe_2O_{3(s)} + CO_{(g)} \rightleftharpoons 2Fe_3O_{4(s)} + CO_{2(g)} \quad \Delta H^o_{1123\,K} = -40.8\ \text{kJ mol}^{-1} \tag{R1}$$

$$Fe_3O_{4(s)} + CO_{(g)} \rightleftharpoons 3FeO_{(s)} + CO_{2(g)} \quad \Delta H^o_{1123\,K} = 9.8\ \text{kJ mol}^{-1} \tag{R2}$$

$$FeO_{(s)} + CO_{(g)} \rightleftharpoons Fe_{(s)} + CO_{2(g)} \quad \Delta H^o_{1123\,K} = -16.5\ \text{kJ mol}^{-1} \tag{R3}$$

Steam reactor (SR):

$$3FeO_{(s)} + H_2O_{(g)} \rightleftharpoons Fe_3O_{4(s)} + H_{2(g)} \quad \Delta H^o_{1123\,K} = -43.4\ \text{kJ mol}^{-1} \tag{R4}$$

$$3Fe_{(s)} + 4H_2O_{(g)} \rightleftharpoons Fe_3O_{4(s)} + 4H_{2(g)} \quad \Delta H^o_{1123\,K} = -94.7\ \text{kJ mol}^{-1} \tag{R5}$$

Air reactor (AR):

$$2Fe_3O_{4(s)} + 0.5O_{2(g)} \rightleftharpoons 3Fe_2O_{3(s)} \quad \Delta H^o_{1123\,K} = -237.2\ \text{kJ mol}^{-1} \tag{R6}$$

The CLHG process has many advantages: (i) inherent CO_2 separation; (ii) thermal neutrality; and (iii) reduced economic sensitivity to process scale. However, one of the major challenges of hydrogen production by chemical looping is the development of an oxygen carrier with high activity that is resistant to mechanical and chemical degradation by attrition, agglomeration, and fragmentation. When the almost pure iron oxide is used as an oxygen carrier, a rapid deactivation is found for the reduction of Fe_3O_4 to Fe within the first few cycles [15]. Limiting the extent of Fe_2O_3 reduction to FeO in every redox cycle, the cyclic stability for hydrogen production could be improved to some extent, but the transition from Fe to Fe_3O_4 produces approximately four times the hydrogen yield compared to the conversion of FeO to Fe_3O_4 [8]. Thus, the reduction from Fe_2O_3 to Fe is more conducive for hydrogen production. To improve the performances of oxygen carriers, inert supports such as Al_2O_3, $MgAl_2O_4$, ZrO_2, SiO_2, and YSZ could provide a larger surface area for reaction and act as an effective binder to increase the oxygen carrier's mechanical strength and attrition resistance [16–21]. It is also reported that incorporating iron with other elements such as Ti, La, Ce, and Sr could improve the cyclic stability of iron-based oxygen carriers and enhance the O^{2-} diffusivity [7,22–26].

More recently, Ca-Fe based catalysts have been of particular interest due to their potential in chemical looping processes [27]. Calcium ferrite is environmentally safe, chemically stable, cheap, and abundant [28]. The mixed phase of $Ca_2Fe_2O_5$ and Fe_2O_3 was used by Zamboni et al. for hydrogen production from toluene steam reforming and has been shown to contribute to the catalytic activity of Fe/CaO systems [29]. Ismail et al. prepared mixed oxides from CaO and Fe_2O_3 by using a simple mixing method and a wet impregnation method [27,30]. It has also been demonstrated that synthesized Ca-Fe based oxygen carriers have an increased capacity for hydrogen production. Martin et al. demonstrated that reduced $Ca_2Fe_2O_5$ produces more hydrogen from steam compared to unmodified Fe and a 75% conversion of steam to hydrogen was achieved with applied $Ca_2Fe_2O_5$ [31]. Kimura et al. performed in

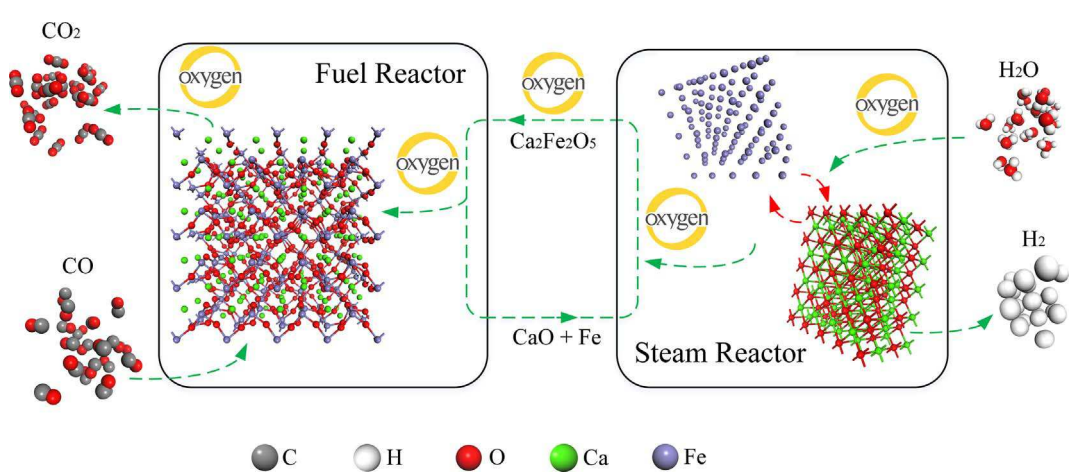

Fig. 1. Schematic of two-step chemical looping hydrogen generation (TCLHG) process using $Ca_2Fe_2O_5$ as an oxygen carrier compared with traditional chemical looping hydrogen generation process.

situ QXAFS experiments on the reduction of Fe_2O_3 and $CaFe_2O_4$ and investigated their reduction mechanisms. The reduction of Fe in $CaFe_2O_4$ was inferred to be a simple first-order reaction [32]. However, the research regarding $Ca_2Fe_2O_5$ and $CaFe_2O_4$ on chemical looping technologies have not been studied sufficiently.

In this study, the possibility of using $Ca_2Fe_2O_5$ and $CaFe_2O_4$ as oxygen carriers for the proposed TCLHG process is further investigated. The schematic diagram of the proposed two-step chemical looping hydrogen generation (TCLHG) process is seen in Fig. 1. Take CO as fuel and $Ca_2Fe_2O_5$ as an oxygen carrier, the two-step chemical looping hydrogen generation (TCLHG) process can be described as:

Fuel Reactor (FR):

$$Ca_2Fe_2O_{5(s)} + 3CO_{(g)} \rightleftharpoons 2CaO_{(s)} + 2Fe_{(s)} + 3CO_{2(g)} \quad \Delta H^o_{1123\,K} = 7.1\ \text{kJ mol}^{-1} \tag{R7}$$

Steam Reactor (SR):

$$2CaO_{(s)} + 2Fe_{(s)} + 3H_2O_{(g)} \rightleftharpoons Ca_2Fe_2O_{5(s)} + 3H_{2(g)} \quad \Delta H^o_{1123\,K} = -107.9\ \text{kJ mol}^{-1} \tag{R8}$$

Take CO as fuel and $CaFeO_4$ as an oxygen carrier, the TCLHG is depicted as:

Fuel Reactor (FR):

$$CaFe_2O_{4(s)} + 3CO_{(g)} \rightleftharpoons CaO_{(s)} + 2Fe_{(s)} + 3CO_{2(g)} \quad \Delta H^o_{1123\,K} = 36.2\ \text{kJ mol}^{-1} \tag{R9}$$

Steam Reactor (SR): Occurred at an ideal situation

$$CaO_{(s)} + 2Fe_{(s)} + 3H_2O_{(g)} \rightleftharpoons CaFe_2O_{4(s)} + 3H_{2(g)} \quad \Delta H^o_{1123\,K} = -98.8\ \text{kJ mol}^{-1} \tag{R10}$$

Steam Reactor (SR): Occurred according to the experimental results

$$CaO_{(s)} + 2Fe_{(s)} + 17/6H_2O_{(g)} \rightleftharpoons 1/2Ca_2Fe_2O_{5(s)} + 1/3Fe_3O_{4(s)} + 17/6H_{2(g)} \quad \Delta H^o_{1123\,K} = -85.5\ \text{kJ mol}^{-1} \tag{R11}$$

This work focuses on (1) the effect of different preparation conditions on the performance of oxygen carriers; (2) the viability of calcium ferrite-based TCLHG processes with inherent CO_2 capture; (3) the cyclic stability and evolution of oxygen carriers' composition; (4) and carbon deposition on $Ca_2Fe_2O_5$ and $CaFe_2O_4$ samples. Multiple cycles of CO reduction-O_2 oxidation and CO reduction-H_2O oxidation experiments were carried out by using $Ca_2Fe_2O_5$ and $CaFe_2O_4$ to assess the long-term activity of oxygen carriers as well as evaluate the capability of producing higher yields of hydrogen compared with the three-step chemical looping hydrogen generation process using Fe_2O_3.

2. Experimental

2.1. Preparation of Ca-Fe based oxygen carriers

$Ca_2Fe_2O_5$ and $CaFe_2O_4$ were prepared by the citric acid assisted sol-gel method. In this process, $Ca(NO_3)_2{\cdot}4H_2O$ (Sigma-Aldrich No.13477-34-4), $Fe(NO_3)_3{\cdot}9H_2O$ (Sigma-Aldrich No.7782-61-8), and citric acid (Sigma-Aldrich No.77-92-9) were mixed according to desired molar ratios (Fe: Ca: citric acid = 1:1:6 for $Ca_2Fe_2O_5$ and Fe: Ca: citric acid = 2:1:9 for $CaFe_2O_4$ preparation) before the mixture was dissolved in deionized water and stirred constantly for 30 min at 40 °C. The solution was then dried at 180 °C for 12 h, followed by calcination in air in a muffle furnace at 650 °C for 4 h (temperature ramp 5 °C/min from room temperature to 650 °C). The effect of preparation parameters (the molar ratios of Fe: Ca: citric acid, drying temperatures, and calcination temperatures) on the physical properties of Ca-Fe based oxygen carriers can be seen in Figs. S1–S4.

2.2. Characterization of carrier materials

To characterize the crystalline phases in the oxygen carrier samples, X-ray powder diffraction (XRD) were conducted by a Rigaku Smartlab diffractometer with applied Cu Kα radiation source, operated at 40 kV and 40 mA. The angle of reflection, 2θ, was varied between 10 and 85°. The BET surface areas were calculated by the BET method from N_2 sorption isotherms recorded at −196 °C using a Quantachrome. All the samples were evacuated at 150 °C for 3 h before N_2 adsorption and desorption isotherms test.

Scanning electron microscopy (SEM) and energy dispersive spectrometer (EDS) were conducted using an FEI Quanta FEG 450 Scanning Electron Microscope with an acceleration voltage of 20 kV and spot size of 4–7. The oxygen carriers were investigated by high-resolution transmission electron microscopy (HRTEM) using an FEI Tecnai G2 F20 S-Twin at 200 kV. The sample powders were dispersed in ethanol under sonication treatment for 3 h. The suspension was then dropped onto a copper grid-supported transparent carbon foil and dried in the ambient atmosphere for several minutes. X-ray photoelectron spectroscopy (XPS) was tested using a Thermo-scientific ESCALAB 250 instrument to determine the states of prepared oxygen carriers. A monochromatic Al Kα was used as an X-ray source with spot size 500 μm, survey scans at 150 eV, composition scans at 20 eV, and low-energy electron flood for charge neutralization.

Temperature-programmed reduction (TPR) was conducted in a quartz reactor equipped with an online mass spectrometer (Hiden, HPR-20 QIC) where 0.1 g of the sample was tested for each run. The oxygen carrier was pre-outgassed by helium at 140 °C for 30 min. The catalyst was cooled to 50 °C while flowing 5% H_2 in N_2 through the sample for 30 min. Then, the H_2-TPR experiment was carried out from 50 °C to 1050 °C with a heating rate of 5 °C/min under a helium atmosphere. Mössbauer measurements were taken at 295 K on a Web Research Co. W100 spectrometer using a 38 mCi ^{57}Co source in rhodium with run times ranging from 24 to 48 h. Spectra were collected in 2048 channels and then all spectral baselines were corrected for the compton scattering of 122 keV gamma rays by electrons inside the detector. The corrected data are equal to A/(1-b), where A is the counts of the uncorrected absorption and b is the Compton fraction determined through recording the counts with and without a 14.4 keV stop filter (~2 mm Al foil) in the gamma ray beam.

2.3. Experimental set-up and procedure

The thermal decomposition performance and O_2 release and storage capacity of the oxygen carrier ($Ca_2Fe_2O_5$ and $CaFe_2O_4$), were carried out by an SDT Q600 TGA. The thermal decomposition experiments were tested by TGA from room temperature to 900 °C at a heating rate of 10 °C/min and an N_2 flow rate of 100 mL/min (Fig. S1). The effect of oxygen carrier type (Fe_2O_3, $Ca_2Fe_2O_5$, and $CaFe_2O_4$), reducing agent type (CO or CH_4), oxygen carrier concentration (5%, 10%, 20%, and 30% with balance N_2), and reduction temperature (800 °C, 850 °C, 900 °C, and 950 °C) were analyzed using TGA by bringing the oxygen carrier to the target temperature and then introducing the specified reducing agent at the specific concentration. The reducing agent flowed past the oxygen carrier surface for 80 minutes before reduction was stopped by stopping the flow of gas across the oxygen carrier surface.

The activity and cyclic stability of $Ca_2Fe_2O_5$ and $CaFe_2O_4$ were studied using a thermogravimetric analyzer (TGA) and a vertical fixed bed reactor. To test the cyclic durability of the oxygen carrier, 20% CO is flowed through the TGA in the CO or CH_4 reduction stage. DI water is provided by a precision syringe pump with a flow rate of 0.01 mL/min during steam oxidation stage. The DI water is heated to a temperature up to 200 °C by a heating tape and mixed with an N_2 flow rate of 120 mL. The mixture of N_2 and steam were then fed into the TGA at the steam oxidation stage. The fixed bed experiments were carried out for XRD, TPR, BET, and SEM characterization of the reacted oxygen

carriers. In a typical experiment, 0.5 g sample was used for multiple cycles of 20% CO reduction and H_2O oxidation with a water injection rate of 0.10 mL/min.

3. Results and discussions

3.1. Physical properties

As seen in Fig. 2, the X-ray diffraction pattern of oxygen carriers prepared by the citric acid assisted sol-gel method (citric acid: Fe: Ca = 3:1:2 and a calcination temperature of 650 °C) confirms the formation of Ca-Fe based oxygen carriers which are mainly composed of $Ca_2Fe_2O_5$ (card 71-2264) and $CaFe_2O_4$ (card 72-1199), respectively. The effect of various citric acid: (Fe + Ca) molar ratios, calcination temperatures, and Fe: Ca ratios on calcium ferrite formation is also investigated as seen in Fig. S2. $Ca_2Fe_2O_5$ could be generated with various composition ratios from 1:1:1 to 4:1:1 as long as the calcination temperature was higher than 650 °C. At temperatures near 550 °C, $CaCO_3$ (card 05-0586) would be formed. It should be noted that higher calcination temperatures lead to sharper peaks of $Ca_2Fe_2O_5$, indicating the growth of the oxide particles under thermal treatment [23].

Effect of Fe: Ca ratios on XRD formation is also investigated. For the oxygen carrier prepared with a composition ratio of Fe: Ca = 0.5, CaO (card 99-0070) and $Ca_2Fe_2O_5$ (card 71-2264) were detected to be the main components. $Ca_2Fe_2O_5$ and $CaFe_2O_4$ could be generated with a Fe: Ca ratios of 1:1 and 1:2, respectively. The diffraction peaks become obscure when the ratio is 4:1 which indicates a low crystallinity and other composite calcium ferrite is formed according to XRD results. Thus, the calcium ferrite compound prepared with composition ratios of 6:1:1 and 9:2:1 at 650 °C are adopted in this study for $Ca_2Fe_2O_5$ and $CaFe_2O_4$ preparation.

The SEM images of the fresh $Ca_2Fe_2O_5$ and $CaFe_2O_4$ with EDS mapping results are also presented in Fig. 2. As can be seen, the $Ca_2Fe_2O_5$ and $CaFe_2O_4$ particles are densely packed and $Ca_2Fe_2O_5$ is more uniformly dispersed than $CaFe_2O_4$. EDS mapping is carried out to analyze the Ca and Fe element distributions. Results reveal that Fe and Ca elements are distributed with a high degree of coincidence, indicating the formation of calcium ferrites $Ca_2Fe_2O_5$ and $CaFe_2O_4$, respectively.

Typical ^{57}Fe-Mössbauer spectra at 295 K measured for $Ca_2Fe_2O_5$ and $CaFe_2O_4$ samples are shown in Fig. 3, where the atomic Fe/Ca ratios of the two samples are 1 and 2, respectively. Hirabayashi et al. have reported a brownmillerite-type $Ca_2Fe_2O_5$ structure with two ferric ion sites of tetrahedral and octahedral from their Mössbauer spectra [28]. As can be seen from Fig. 3, the $Ca_2Fe_2O_5$ sample forms two sets of sextets which occupied octahedral and tetrahedral sites of the brownmillerite-type structure, respectively. It can be concluded that the blue sub-spectrum corresponds to Fe^{3+} in tetrahedral sites and the green sub-spectrum is attributed to Fe^{3+} in the octahedral sites. Mössbauer spectroscopy with a Fe: Ca molar ratio of 2:1 also confirms the presence of the $CaFe_2O_4$ phase [28,33].

The results of BET surface characterizations of Ca-Fe based oxygen carrier are presented in Table 1 and the surface areas of fresh $Ca_2Fe_2O_5$ and $CaFe_2O_4$ are 59.9 m^2/g and 53.1 m^2/g, respectively. The effect of citric acid: (Fe + Ca) molar ratios addition on the BET surface area, pore volume distributions of fresh $Ca_2Fe_2O_5$ and $CaFe_2O_4$ are presented in Fig. S3. With the increase of citric acid in the preparation process, the BET surface area initially increases and then decreases while BJH pore volume remains stable with the citric acid: (Fe + Ca) molar ratio from 1:1 to 3:1. It can also be inferred that the molar ratios of citric acid: (Fe + Ca) at 2:1 or 3:1 are better choices due to a relatively high BET surface area and BJH pore volume distribution. The effect of calcination temperatures and Fe: Ca molar ratios on the performances of oxygen carriers is also investigated as seen in Figs. S4 and S5.

Fig. 4 shows the transmission electron microscope (TEM) micrographs and Energy-dispersive X-ray element mapping of $Ca_2Fe_2O_5$ and $CaFe_2O_4$ samples. A spherical-like structure and a block-like structure were noted from Fig. 4a and b, respectively. The TEM images reveal that the nanoparticle dispersion is relatively uniform. In addition, the particle size of $Ca_2Fe_2O_5$ and $CaFe_2O_4$ are estimated to range from 10 to 20 nm, which is in good agreement with that calculated by the XRD analysis as shown in Table 1, also indicating the TEM results are representative. It is noteworthy that a binding interface is observed between $Ca_2Fe_2O_5$ and $CaFe_2O_4$ samples which could be caused by the crystal cross or overlap due to a strong structural interaction [23]. Electron diffraction patterns (See Fig. 4c and g) show intense light spots, indicating the highly crystalline formation of $Ca_2Fe_2O_5$ and $CaFe_2O_4$ phases [34].

3.2. Reduction activity

3.2.1. Effect of oxygen carriers

The CO reduction performances under different oxygen carriers (Fe_2O_3, $Ca_2Fe_2O_5$, and $CaFe_2O_4$), CO concentration (5%, 10%, 20%,

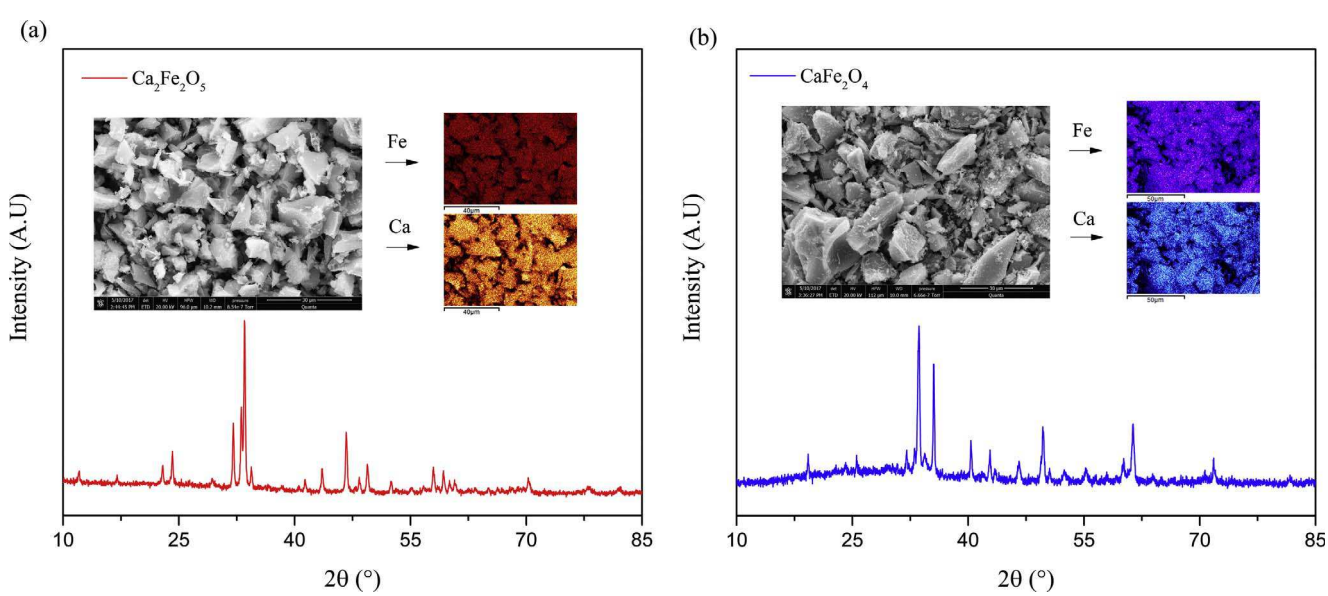

Fig. 2. XRD and corresponding SEM/EDS mapping analysis of: (a) $Ca_2Fe_2O_5$ and (b) $CaFe_2O_4$ samples.

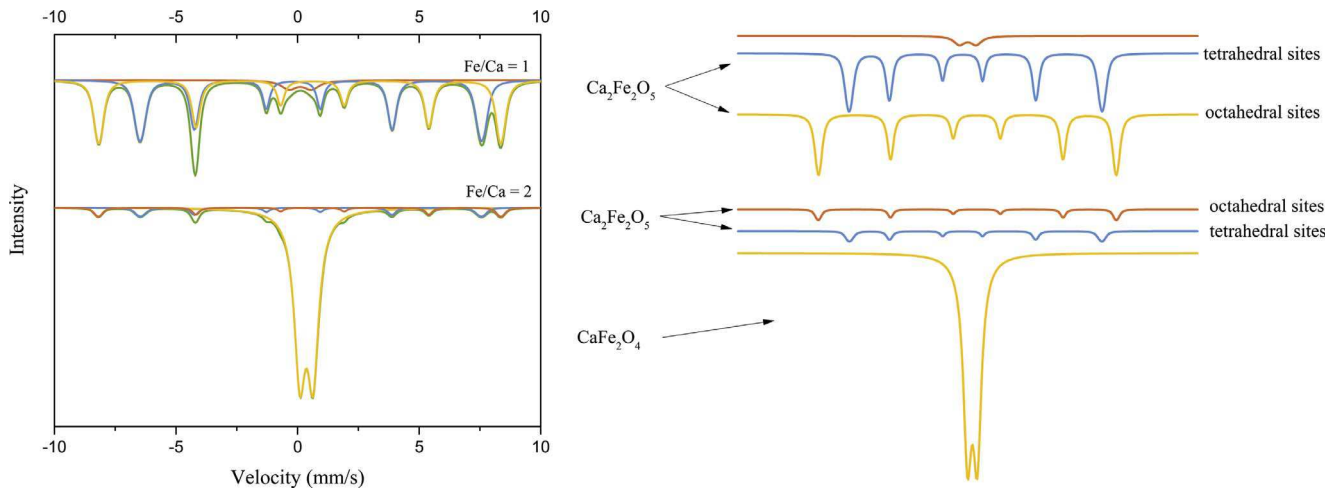

Fig. 3. Mossbauer spectra of $Ca_2Fe_2O_5$ (Fe/Ca = 1) and $CaFe_2O_4$ (Fe/Ca = 2) samples.

Table 1
Physical properties of fresh and reacted Ca-Fe based oxygen carriers.

Oxygen carriers	Crystal size (nm)	Average pore size (nm)	BET surface area (m^2/g)	Pore volume (g/cm^3)
$Ca_2Fe_2O_5$	17.9	7.2	59.9	0.148
$CaFe_2O_4$	13.5	10.1	53.1	0.131
5th Reacted $Ca_2Fe_2O_5$	18.7	3.1	34.3	0.031
5th Reacted $CaFe_2O_4$	14.9	3.7	31.5	0.032
10th Reacted $Ca_2Fe_2O_5$	18.7	4.0	31.2	0.032
10th Reacted $CaFe_2O_4$	15.4	3.9	36.0	0.031

and 30%), and reduction temperatures (800 °C, 850 °C, 900 °C, and 950 °C) are investigated as presented in Fig. 5 and the enlarged figures of the initial stage are provided in Figs. S6–S9. The effect of different oxygen carriers (Fe_2O_3, $Ca_2Fe_2O_5$, and $CaFe_2O_4$) on CO reducibility was studied under the condition of temperature 900 °C and CO concentration 20% (Figs. 5a and S6). For Fe_2O_3, a two-stage reduction could be found. The first-step reduction is fast which α-Fe_2O_3 changed to a FeO-like structure while the second-step reduction becomes slow which involves the reduction of Fe^{2+} to Fe^0 [32]. For the first 5 minutes of the initial reduction stage, all the oxygen carriers show a relatively high activity and $CaFe_2O_4$ performs the highest reduction rate of the three oxygen carriers. With continued CO reduction, the weight loss of three oxygen carriers could be distinguished apparently. $Ca_2Fe_2O_5$ performs the highest weight loss rate and Fe_2O_3 shows the lowest weight loss rate. Thus, the CO reduction activity is summarized as $Ca_2Fe_2O_5$ > $CaFe_2O_4$ > Fe_2O_3 which is consistent with the XRD results as seen in Fig. S10 (H_2-TPR results see Fig. S11). A slight weight increase is found in $CaFe_2O_4$ and $Ca_2Fe_2O_5$ when the mass residue of oxygen carriers reaches their maximum value, indicating the occurrence of carbon deposition. Once the oxygen carrier was completely or tends to be completely reduced, the reducing gas agent (CO) couldn't be oxidized in time, potentially leading to disproportionation reactions.

3.2.2. Effect of reducing agent concentration

The effect of CO concentration (5%, 10%, 20%, and 30%) on reduction reactivity is also explored using $Ca_2Fe_2O_5$ under a temperature of 900 °C. As can be seen from Figs. 5b and S7, the reduction rate increases as CO concentration increases. Concentrations of 20% and 30% are feasible due to a relatively fast reduction rate. Further, a CO concentration of 20% is better than that of 30% due to the less amount of carbon deposition.

3.2.3. Effect of temperatures

The effect of reduction temperatures (800 °C, 850 °C, 900 °C, and 950 °C) on CO reducibility is shown in Figs. 5c and S8. It is noted that increasing temperature leads to faster conversion of CO to CO_2 across the first 4 minutes of reduction, indicating the reduction activity at various temperature is as follows: 950 °C > 900 °C > 850 °C > 800 °C. However, over longer time periods, larger amounts of CO reduction occur at 900 °C performs a slightly higher weight loss compared with that of other temperatures and thus reduction activity is as follows: 900 °C > 950 °C > 850 °C > 800 °C. This is believed to be the case because carbon deposition increases with rising temperature, thus, 900 °C is seen to be the best condition for $Ca_2Fe_2O_5$ reduction of the four tested temperatures due to a higher reduction activity and lower amount of carbon deposition. For $CaFe_2O_4$, temperature shows a promoted effect on CO reduction activity and the reduction rate improves to a greater degree than that on other surfaces with the temperature increasing (Figs. 5d and S9). Since it has been demonstrated that the CO reduction activity is higher on $Ca_2Fe_2O_5$ than on $CaFe_2O_4$, CH_4 reduction experiments were carried out using $Ca_2Fe_2O_5$ as the oxygen carrier at 900 °C with a CH_4 concentration of 20% (Fig. S12).

A weight increase has been observed from both CO and CH_4 reduction when the oxygen carrier approaches to be completely reduced or completely reduced. This may be due to carbon deposition or Fe_3C formation. It has been reported that Fe_3C is produced during CO reduction over using Fe_2O_3 as an oxygen carrier seen from (R12) [22]. Moreover, carbon could be deposited through the Boudouard reaction under certain conditions as seen in (R13). Thus, XRD tests are carried out to clarify if Fe_3C is generated during CO or CH_4 reduction stage. The oxygen carrier is obtained from fixed bed experiments under the conditions of temperatures at 800 °C and 900 °C, reducing agent concentration of 20%, and reduction time of 80 min. The XRD results presented in Fig. 6a confirm that all the CO reduced Ca-Fe based oxygen carriers exist in the form of CaO and Fe and none of the Fe_3C was produced from CO reduction of the fresh $Ca_2Fe_2O_5$ or $CaFe_2O_4$. Thus, the mass increase can be attributed to the carbon deposition from CO disproportionation.

3.2.4. Effect of reducing agent

As for CH_4 reduction experiments (Fig. 6b), CaO, Fe, and $Ca_2Fe_2O_5$ were found to be the main component of CH_4 reduction using $Ca_2Fe_2O_5$ and $CaFe_2O_4$ at 800 °C which could be explained by the low reduction activity, resulting in incomplete oxygen carrier reduction. The incomplete reduction of the oxygen carrier effectively prevented the formation of Fe_3C. For the CH_4 reduction temperature at 900 °C, Fe_3C (card 34-0001) is generated from both $Ca_2Fe_2O_5$ and $CaFe_2O_4$ reduction as seen in Fig. 6. Combined with TGA results (See Fig. S12), it could be

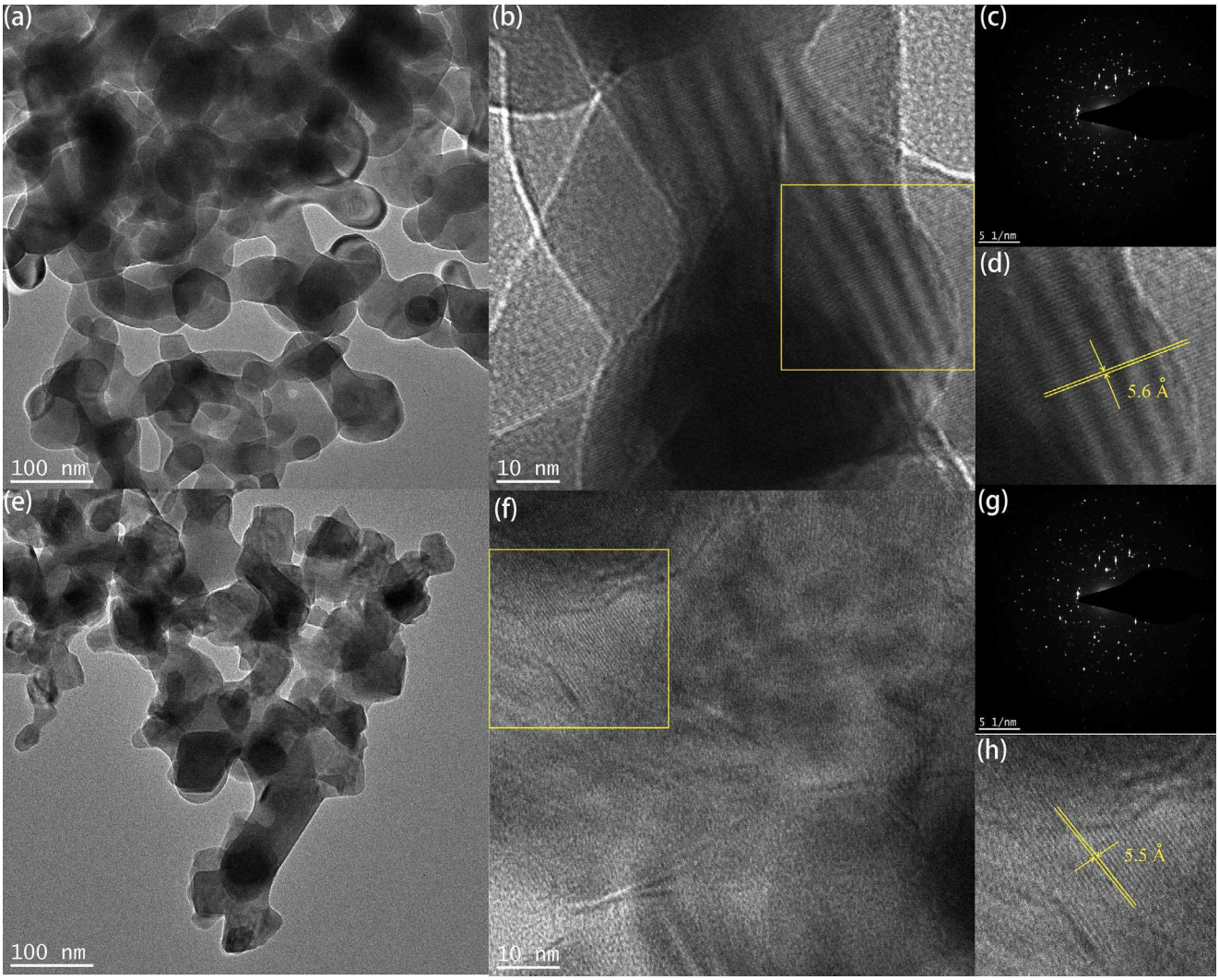

Fig. 4. Representative TEM/HRTEM micrograph of the oxygen carriers: (a) $Ca_2Fe_2O_5$; (b): high-resolution image of $Ca_2Fe_2O_5$; (c): electron diffraction patterns of $Ca_2Fe_2O_5$; (d) crystal size analysis of $Ca_2Fe_2O_5$; (e) $CaFe_2O_4$; (f) high-resolution image of $CaFe_2O_4$; (g) electron diffraction patterns of $CaFe_2O_4$; (h) crystal size analysis of $CaFe_2O_4$.

concluded that once $Ca_2Fe_2O_5$ or $CaFe_2O_4$ is reduced completely or close to be fully reduced, Fe_3C begins to gradually accumulate. However, the mechanism of Fe_3C formation is still not clear and needs to be investigated further.

$$2Fe_3O_{4(s)} + 6CO_{(g)} \rightleftharpoons Fe_3C_{(s)} + 5CO_{2(g)} \quad \Delta H^o_{1123\,K} = -194.5\ \text{kJ mol}^{-1} \tag{R12}$$

$$2CO_{(g)} \rightleftharpoons C_{(s)} + CO_{2(g)} \quad \Delta H^o_{1123\,K} = -169.4\ \text{kJ mol}^{-1} \tag{R13}$$

3.3. Cyclic reduction and oxidation

Multiple cycles of O_2 release and storage experiments were performed with applied TGA at a representative temperature of 900 °C using CO and CH_4 as reducing agent. Detailed profiles are provided in Fig. S13. The O_2 carrying capacity of the oxygen carriers can be evaluated by the oxygen ratio Ro, which is defined as $R_o = (m_{ox} - m_{red})/m_{ox}$ [35,36] . According to the definition, the theoretical O_2 carrying capacity of Fe_2O_3 (Fe_3O_4), $Ca_2Fe_2O_5$, and $CaFe_2O_4$ are calculated which are 0.276, 0.176, and 0.222, respectively. When Fe_2O_3 is adopted as an oxygen carrier, the final steam oxidized phase would be Fe_3O_4 instead of Fe_2O_3. It is found that the O_2 carrying capacity of $Ca_2Fe_2O_5$ and $CaFe_2O_4$ is lower than Fe_2O_3. This is because CaO does not participate in the redox reactions. Both $Ca_2Fe_2O_5$ and $CaFe_2O_4$ possess excellent cyclic stability using CO reducing agent and no appreciable decrease in O_2 carrying capacity could be observed over 10 cycles of chemical looping combustion (CLC). As for $CaFe_2O_4$, however, the O_2 release and storage capacity decreases after the 8th redox cycle with CH_4. A weight increase could be found due to carbon deposition and subsequent Fe_3C formation during the post-reduction stage.

According to the results of CO and CH_4 reduction experiments, temperatures of 900 °C and CO concentration of 20% has been shown to be favorable for the fast and complete reduction of $Ca_2Fe_2O_5$ and $CaFe_2O_4$ with less carbon deposition. Therefore, the cyclic stability of $Ca_2Fe_2O_5$ and $CaFe_2O_4$ is tested with CO reduction and steam oxidation at 900 °C and CO concentration of 20%. Each redox cycle consists of four stages: (1) reduction (30 min), (2) N_2 purification (10 min), (3) steam oxidation (3 min), and (4) N_2 purification (17 min). The results of weight change (%) and redox conversion of $Ca_2Fe_2O_5$ and $CaFe_2O_4$, as well as hydrogen concentration over multicycles of reduction-oxidation reaction, are presented in Fig. 7. The results demonstrate that the durability of two Ca-Fe based oxygen carriers is basically unchanged after 20 cycles of repeated CO reduction and H_2O oxidation.

The conversion of the two oxygen carriers, seen in Fig. 7c, is calculated as the ratio of actual weight loss to the weight loss of complete reduction to Fe and CaO, resulting in average conversions of 94.0% and 85.5% for $Ca_2Fe_2O_5$ and $CaFe_2O_4$, respectively. The lower conversion of $CaFe_2O_4$ compared with $Ca_2Fe_2O_5$ can be explained by the lower

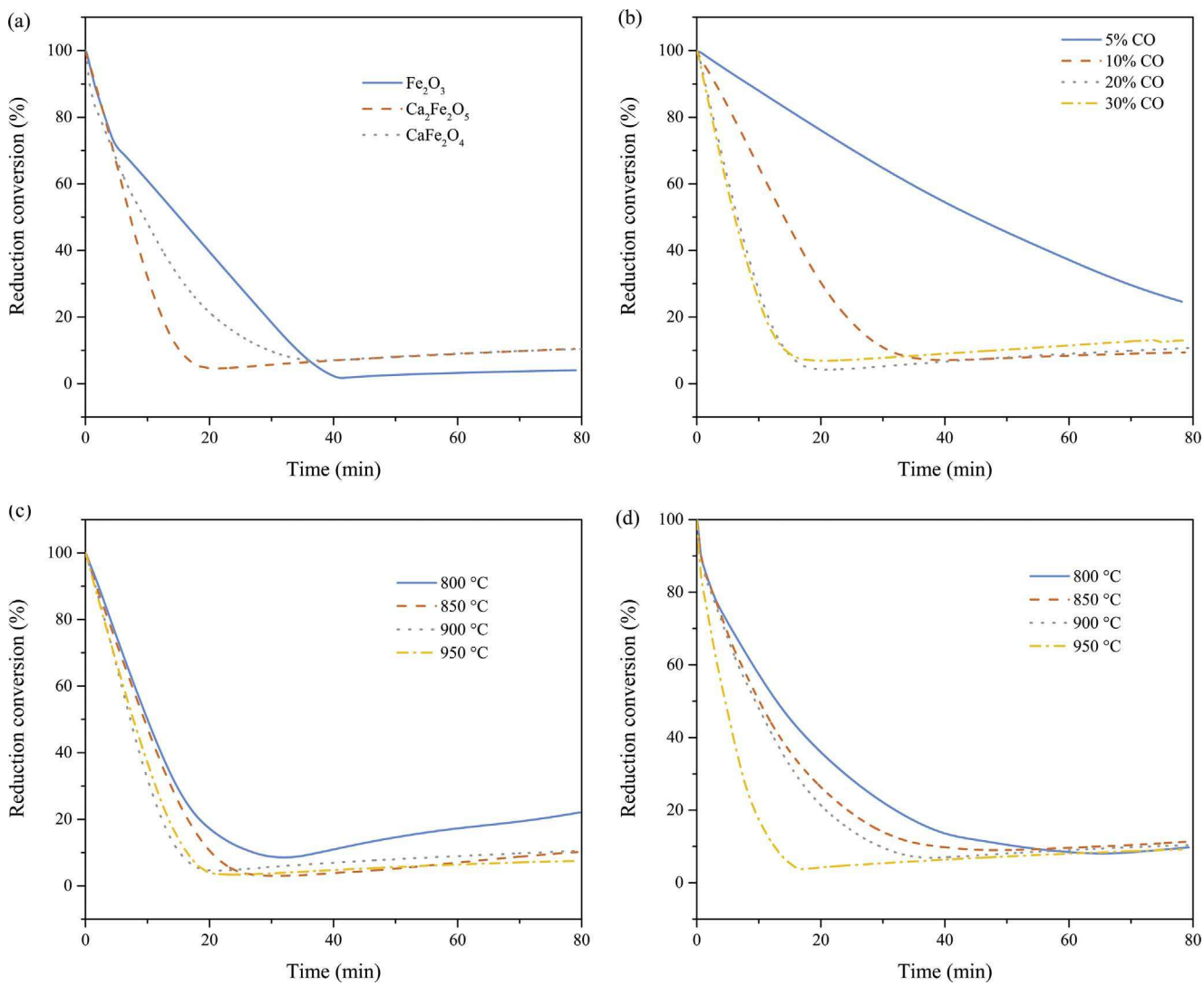

Fig. 5. Oxygen carrier reduction residue (%) as a function of reaction time: (a) investigation on CO reducibility of different oxygen carriers (Fe_2O_3, $Ca_2Fe_2O_5$, $CaFe_2O_4$) under the condition of temperature 900 °C and CO concentration 20 %; (b) effect of CO concentration (5 %, 10 %, 20 %, and 30 %) on the reduction reactivity of $Ca_2Fe_2O_5$ sample at 900 °C; (c) effect of reduction temperatures (800 °C, 850 °C, 900 °C, and 950 °C) on $Ca_2Fe_2O_5$ reduction reactivity under the CO concentration of 20%; (d) effect of reduction temperatures (800 °C, 850 °C, 900 °C, and 950 °C) on $CaFe_2O_4$ reduction reactivity under a CO concentration of 20%.

reduction activity which leads to an incomplete reduction of $CaFe_2O_4$ in a limited reduction time, and 2) the formation of Fe_3O_4 which reduces the O_2 carrying capacity. The phase changes of oxygen carriers over multiple redox cycles as seen in Fig. 8 (a: $Ca_2Fe_2O_5$; b: $CaFe_2O_4$). The XRD patterns show the evolution experienced during CO reduction, H_2O oxidation, the 5th redox reaction, and the 10th redox reaction. The stability of $Ca_2Fe_2O_5$ is demonstrated by its continued existence across 10 redox cycles, whereas $CaFe_2O_4$ sample forms $Ca_2Fe_2O_5$ and Fe_3O_4 (card 89-0688) as the main components of the oxygen carrier after the first redox cycle. $Ca_2Fe_2O_5$ and $CaFe_3O_5$ (card 31-0274) were further formed at the 5th redox cycle as seen in Fig. 8b. Thus, $Ca_2Fe_2O_5$ and $CaFe_3O_5$ are concluded to be the stable crystalline phases after several cycles of CO reduction and H_2O oxidation. Possible redox reactions for $CaFe_3O_5$ are concluded to be as follows:

$CaFe_3O_5$ reduction:

$$CaFe_3O_{5(s)} + 4CO_{(g)} \rightleftharpoons CaO_{(s)} + 3Fe_{(s)} + 4CO_{2(g)} \quad \Delta H^o_{1123\,K} = 36.18\ \text{kJ mol}^{-1} \tag{R14}$$

$CaFe_3O_5$ formation:

$$CaO_{(s)} + 3Fe_{(s)} + 4H_2O_{(g)} \rightleftharpoons CaFe_3O_{5(s)} + 4H_{2(g)} \quad \Delta H^o_{1123\,K} = -98.84\ \text{kJ mol}^{-1} \tag{R15}$$

According to the Ca: Fe molar ratio (Ca: Fe = 0.5) used in the preparation process, the generated $CaFe_3O_5$ has twice as many moles as $Ca_2Fe_2O_5$. The iron utilization efficiency is decreased by 8.33% compared with pure $Ca_2Fe_2O_5$ but still 3.03% higher than that of Fe_2O_3 assuming that all oxygen carriers are completely reduced. Thus, the decrease of $CaFe_2O_4$ conversion from the 1st to 2nd cycle, as seen in Fig. 7c, could be attributed to the formation of Fe_3O_4 or $CaFe_3O_5$ and leads to the oxygen carrier conversion decreasing.

TCLHG experiments were also carried out using a fixed bed reactor over 10 cycles to detect the cyclic hydrogen concentration. As seen in Fig. 7d, TCLHG cycle experiments demonstrated that the hydrogen concentration at the first cycle is lower than that of cycles 2–10. This can be explained by the XPS results that carbon and $CaCO_3$ were formed at the surface of $Ca_2Fe_2O_5$ and $CaFe_2O_4$ during the preparation process (Figs. S14 and S15). The deposited carbon will react with steam releasing CO and the deposited $CaCO_3$ during the reduction stage will also release CO_2 according to reaction (R16) and (R17), shown below.

$$C_{(s)} + H_2O_{(g)} \rightleftharpoons CO_{(g)} + H_{2(g)} \quad \Delta H^o_{1123\,K} = 135.75\ \text{kJ mol}^{-1} \tag{R16}$$

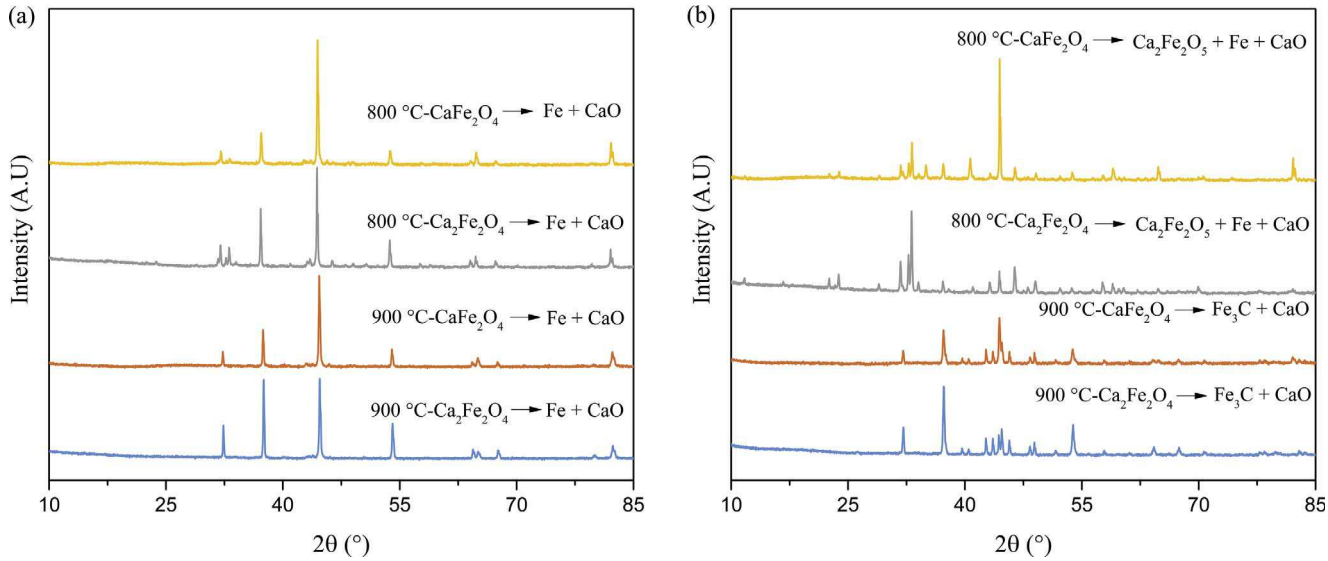

Fig. 6. XRD patterns of reduced oxygen carriers ($Ca_2Fe_2O_5$ and $CaFe_2O_4$) under the condition that the reduction temperature is at 800 °C and 900 °C, the concentration of CH_4 and CO is 20%, and the reduction time is 80 min: (a) CO and (b) CH_4 as reducing agent.

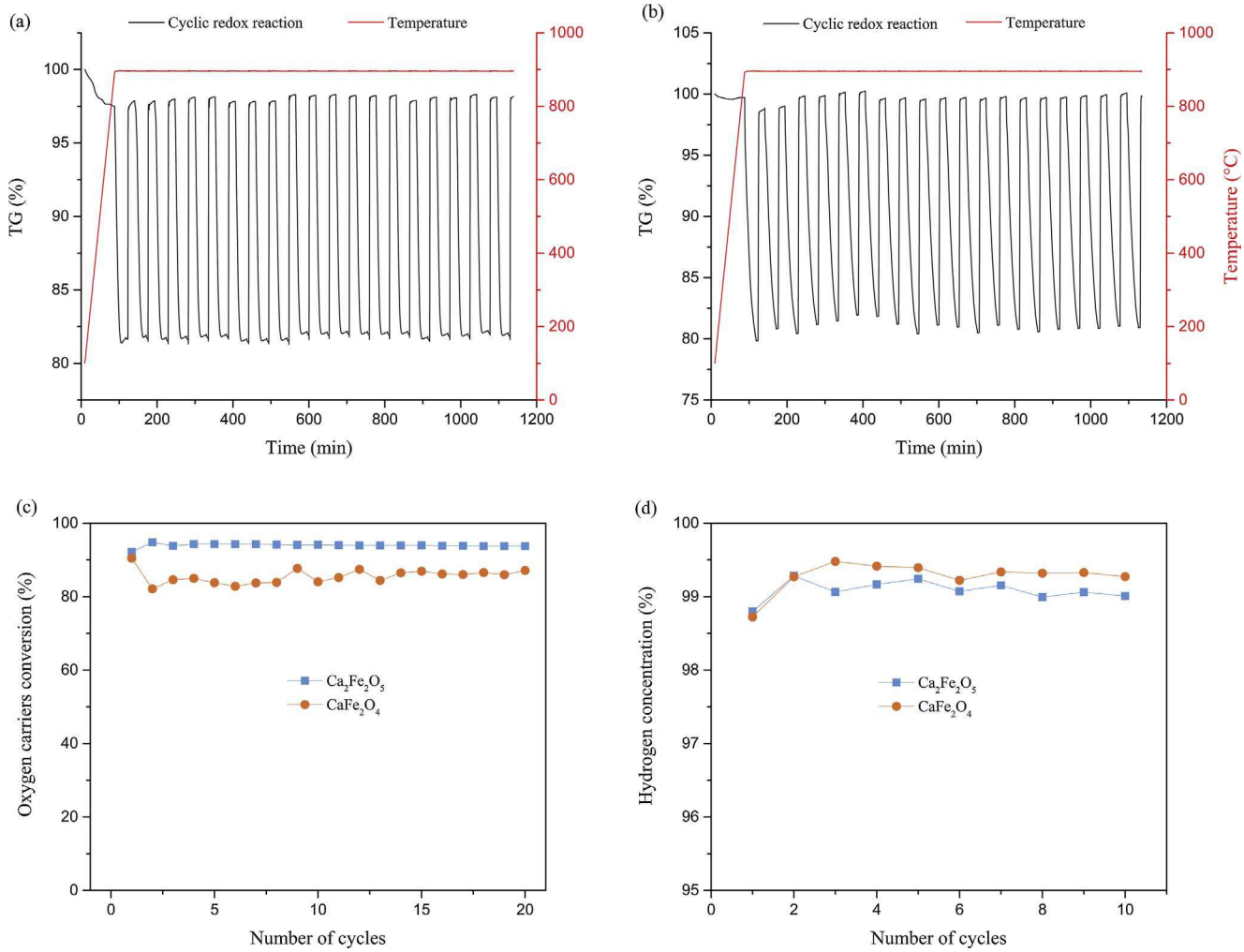

Fig. 7. Investigation on the cyclic reaction performances of oxygen carriers using CO and H_2O as reducing and oxidizing agent at 900 °C under a CO concentration of 20%: (a) TGA data for 20-cycle CLHG experiment using $Ca_2Fe_2O_5$ as oxygen carrier; (b) TGA data for 20-cycle CLHG experiment using $CaFe_2O_4$ as oxygen carrier; (c) conversion of oxygen carriers as a function of the number of cycles; and (d) hydrogen concentration for the first 10 cycles using a fixed bed reactor.

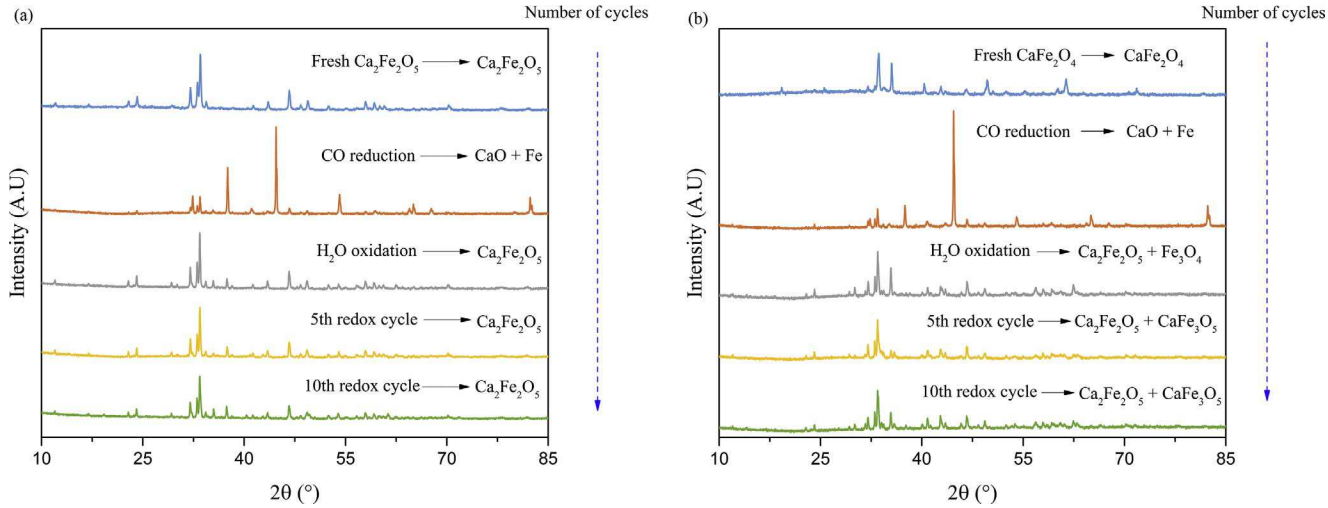

Fig. 8. Phase changes of oxygen carriers over multiple redox cycles: (a) XRD patterns of fresh, CO reduced, H_2O oxidized, 5th reacted, and 10th reacted $Ca_2Fe_2O_5$ sample; (b) XRD patterns of fresh, CO reduced, H_2O oxidized, 5th reacted, and 10th reacted $CaFe_2O_4$ sample.

$$CaCO_{3(s)} \rightleftharpoons CO_{2(g)} + CaO_{(s)} \quad \Delta H^{o}_{1123\,K} = 166.58\ \text{kJ mol}^{-1} \tag{R17}$$

The produced CO_2 and CO gas lead to a relatively low hydrogen concentration. With the number of cycles, the hydrogen concentration remains relatively stable and is basically more than 99% for both $Ca_2Fe_2O_5$ and $CaFe_2O_4$. It has been shown that the CO reduction performance on $Ca_2Fe_2O_5$ is higher than that of $CaFe_2O_4$ and the time required to complete reduction of $Ca_2Fe_2O_5$ was shorter than that of $CaFe_2O_4$. $Ca_2Fe_2O_5$ experiences extended periods of carbon deposition which leads to a lower hydrogen concentration. By adjusting a suitable reduction time, a higher hydrogen concentration could be obtained with applied $Ca_2Fe_2O_5$ as the oxygen carrier of the TCLHG process.

The evolution of BET surface area and BJH pore volume of $Ca_2Fe_2O_5$ and $CaFe_2O_4$ over multiple redox cycles are illustrated in Figs. 9 and S16. The redox reaction occurs under a high operating temperature (900 °C) inevitably sinters the particles and eliminates partial micro or mesoporous structures of the oxygen carriers [24], thus the initial BET surface area and pore volume of the fresh samples are higher than that of reacted oxygen carriers. As can be seen in Fig. 9a, the BET surface area and pore volume of $Ca_2Fe_2O_5$ decreased with the number of cycles then remained relatively constant after multiple cycles of the redox reaction. For $CaFe_2O_4$ (Fig. 9b), which produces $CaFe_3O_5$ and $Ca_2Fe_2O_5$ over multiple redox cycles, the BET surface area of reacted $CaFe_2O_4$ slightly increases, but the pore volume of reacted $CaFe_2O_4$ keeps stable (Fig. 9b).

The SEM images of the 10th reacted $Ca_2Fe_2O_5$ and $CaFe_2O_4$ are shown in Fig. 10. After multicycles of CO reduction and steam oxidation, $Ca_2Fe_2O_5$ and $CaFe_2O_4$ samples had morphological changes and both reacted oxygen carriers showed partial sintering and agglomeration which leads to slight decreases in pore size and volume. Moreover, the surface of the reacted oxygen carriers became less dense. Combined with the BET surface and BJH pore volume results of SEM imaging, the reacted oxygen carriers were concluded to be more stable.

A comparison of CO reduction and H_2O oxidation of $Ca_2Fe_2O_5$ (Fig. 11a and c) and $CaFe_2O_4$ (Fig. 11b and d) shows the conversion rate of $Ca_2Fe_2O_5$ for the first cycle is lower than later cycles, which is attributed to incomplete oxidation of the fresh oxygen carriers. It is also found from Fig. 11a that the $Ca_2Fe_2O_5$ conversion remains stable over multiple redox cycles which indicates significant stability of $Ca_2Fe_2O_5$. Although the decreasing pore volume of the reacted oxygen carriers would reduce the capability of gas diffusion and penetration, the impact of pore volume deterioration on the reduction activity of the oxygen carriers is not that obvious [9,20]. The steam oxidation process could possibly reactivate the oxygen carriers and reduce the amount of carbon deposition after each reduction stage. Both $Ca_2Fe_2O_5$ and $CaFe_2O_4$ maintain a relatively stable conversion rate over multiple redox cycles. However, it should be noted that the reduction and oxidation conversion rates of $CaFe_2O_4$ are both lower than that of $Ca_2Fe_2O_5$. The conversion of the reacted $CaFe_2O_4$ is also decreased compared with the first $CaFe_2O_4$ reduction cycle but performs increases slightly as the number of redox cycles increases, and the progression of reduction activity

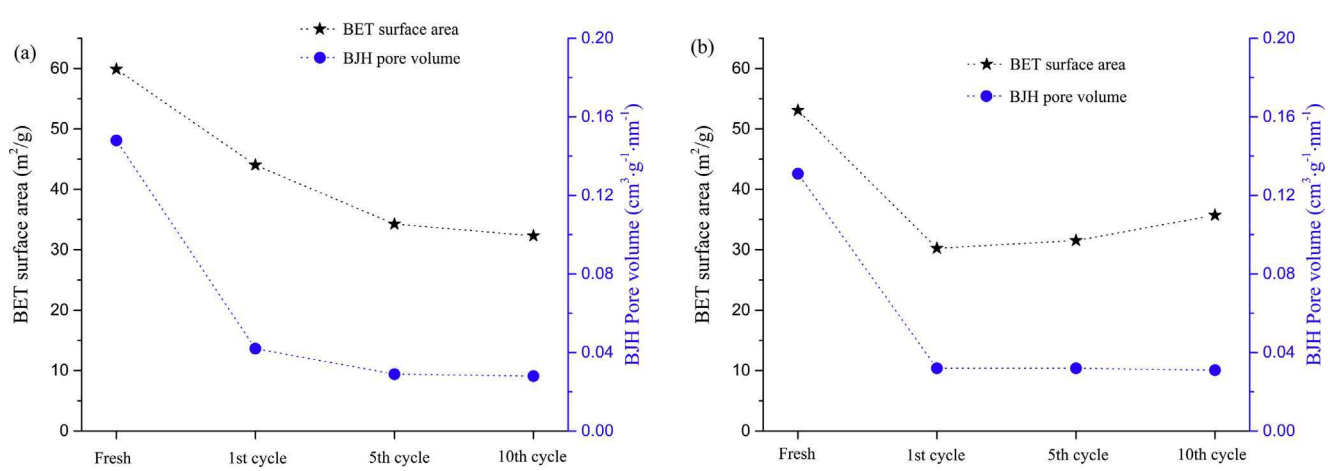

Fig. 9. BET surface area and BJH pore volume changes for Ca-Fe based oxygen carriers over multiple redox cycles: (a) $Ca_2Fe_2O_5$; (b) $CaFe_2O_4$.

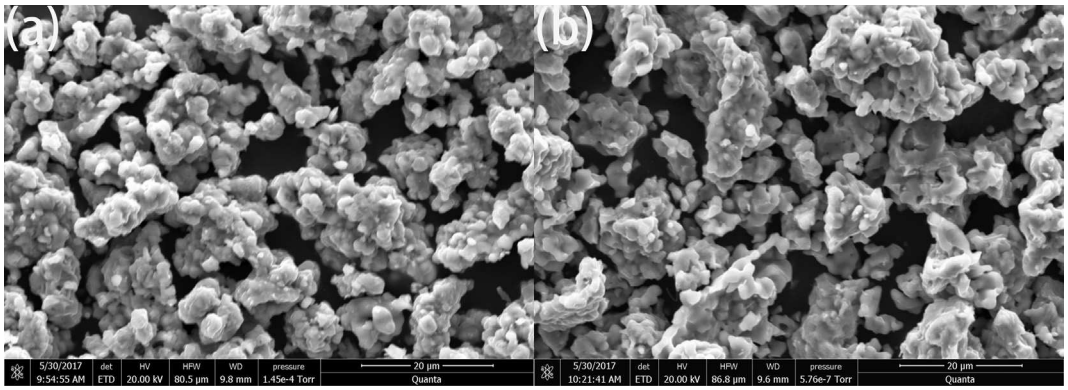

Fig. 10. SEM images of Ca-Fe based oxygen carriers after 10 cycles of redox reaction: (a) $Ca_2Fe_2O_5$; (b) $CaFe_2O_4$.

follows 1st cycle > 20th cycle > 15th cycle > 10th cycle > 5th cycle. These results are consistent with the XRD phase changes from Fig. 8b. The reacted $CaFe_2O_4$ ($Ca_2Fe_2O_5$ and $CaFe_3O_5$) couldn't be completely oxidized which leads to a decrease in conversion. Furthermore, the reduction performances of the reacted $CaFe_2O_4$ increased, possibly due to steam reactivation during oxidation. Thus, it could be concluded that $Ca_2Fe_2O_5$ still shows higher activity and stability than that of $CaFe_2O_4$.

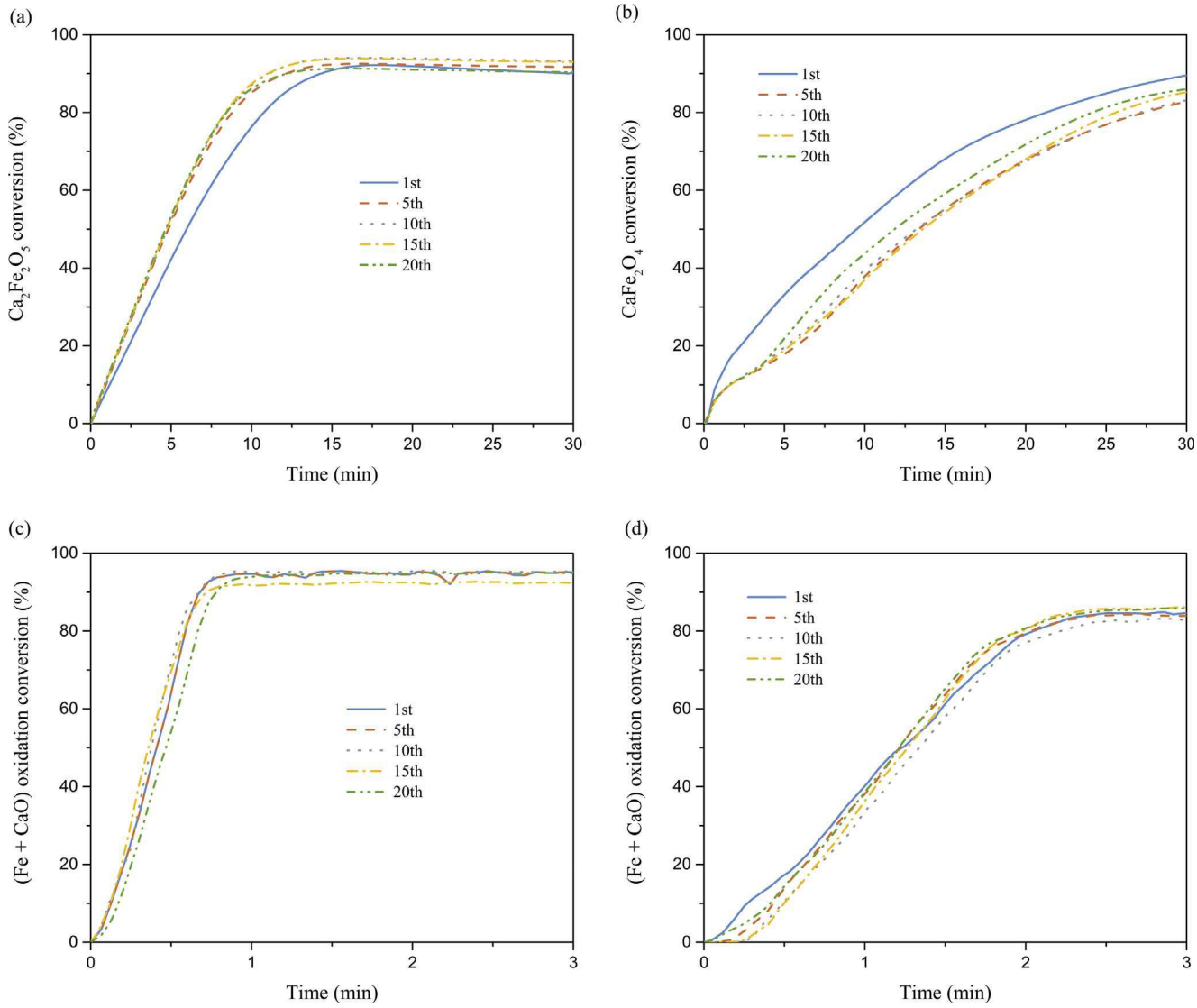

Fig. 11. Relationships between conversion of oxygen carriers and reaction time using CO as the reducing agent and H_2O as oxidizing agent over multiple redox cycles: (a) $Ca_2Fe_2O_5$ reduction; (b) $CaFe_2O_4$ reduction; (c) reduced $Ca_2Fe_2O_5$ oxidation; (d) reduced $CaFe_2O_4$ oxidation.

4. Discussion

4.1. Oxidation process

For three-step chemical looping hydrogen generation processes, iron oxide or modified iron oxide is generally used as an oxygen carrier which circulates among the CLHG reactors to produce hydrogen. However, the highest possible degree of H_2O-oxidation converts Fe to Fe_3O_4 instead of Fe_2O_3. Thus, an air reactor (AR) is needed to make sure the regeneration from Fe_3O_4 to Fe_2O_3, resulting in the net reaction for the three-step CLHG process shown in (R18), below.

$$CO + xH_2O + (1-x)/2O_2 \rightarrow CO_2 + xH_2 \quad \text{(R18)}$$

In (R18), x represents the reduction degree of Fe_2O_3 which is ranged from 0 to 8/9. x = 8/9 means that all Fe_2O_3 in the iron-based oxygen carrier was reduced to Fe [37]. Thus, the completely CO reduction reaction can be described as:

$$CO + 8/9H_2O + 1/18O_2 \rightarrow CO_2 + 8/9H_2 \quad \text{(R19)}$$

As for the proposed two-step chemical looping hydrogen generation (TCLHG) process, it has been proved to be feasible using a calcium ferrite oxygen carrier ($Ca_2Fe_2O_5$). Further, a complete steam oxidation from Fe^0 to Fe^{3+} has been guaranteed to be achievable. Thus, the CLHG process becomes less complicated due to the elimination of AR. It is also expected that more hydrogen will be generated with same moles of iron addition. Thus, the net reaction for TCLHG process would be:

$$CO + H_2O \rightarrow CO_2 + H_2 \quad \text{(R20)}$$

Comparing (R19) and (R20), the TCLHG process is seen to produce higher yields of hydrogen with inherent CO_2 separation by using a fuel reactor and a steam reactor. The hydrogen yields are expected to increase by 12.5% with equivalent moles of Fe in the oxygen carrier and complete reduction from Fe^{3+} to Fe^0. In addition, CO_2 production, which depends on the activity between the oxygen carrier and fuel, is equivalent if the fuel is fully oxidized by the oxygen carrier.

4.2. Reduction process

The CO reduction performances of oxygen carriers (Fe_2O_3, $Ca_2Fe_2O_5$, and $CaFe_2O_4$) for chemical looping hydrogen generation has been investigated for comparison. $Ca_2Fe_2O_5$ and $CaFe_2O_4$ show better performances than that of Fe_2O_3 and the reduction performances of the three catalysts as follows: $Ca_2Fe_2O_5 > CaFe_2O_4 > Fe_2O_3$. The effect of CO concentration and reduction temperatures is also studied to select a better condition for TCLHG process. Higher reducing agent concentration promoted the reduction rate but also led to increased carbon deposition. A CO concentration of 20% was shown to have the best performance as it balances reduction and carbon deposition rates. As for the temperature, higher reduction temperatures promoted reduction activity and reduced carbon deposition, but high-temperature operation accelerated sintering and agglomeration of the oxygen carriers and consumed more energy. Thus, temperatures of 850 °C performed best.

The CH_4 reduction experiments are carried out to compare the performances of different reducing agents at 900 °C and a reducing agent concentration of 20%. $Ca_2Fe_2O_5$ and $CaFe_2O_4$ were reduced to a similar degree using CH_4, but both were reduced significantly less with CH_4 compared to CO. Once the oxygen carrier is completely reduced or closed to be completely reduced by CH_4, a rapid mass increase was observed due to carbon deposition and Fe_3C formation. Some solutions are provided to avoid or reduce the Fe_3C production during CH_4 reduction stage: 1) Adopting appropriate reduction conditions such as CH_4 concentration, temperatures, and reduction time or partially oxidizing CH_4 or CH_4-containing syngas not only could avoid the production of Fe_3C but may also provide the required heat for TCLHG process.

5. Conclusions

A novel chemical looping application is reported: a two-step chemical looping hydrogen generation (TCLHG) process which achieves complete oxidation from Fe^0 to Fe^{3+} using the citric acid assisted sol-gel method for preparing $Ca_2Fe_2O_5$ and $CaFe_2O_4$ as oxygen carriers. The effect of different preparation conditions on the crystalline structure, specific surface area, and BJH pore volume distribution was investigated. Conditions of Citric acid: (Fe + Ca) molar ratio 3:1, drying temperature 180 °C, and calcination temperature 650 °C were proved to be feasible and adopted for $Ca_2Fe_2O_5$ and $CaFe_2O_4$ preparation.

The experiments presented in this study verified that calcium ferrite is feasible as an oxygen carrier in the proposed TCLHG process. Thermogravimetric analysis results indicate that the oxygen carriers, especially $Ca_2Fe_2O_5$, show high CO reduction and steam oxidation activity as well as cyclic durability. The conversion of $Ca_2Fe_2O_5$ and $CaFe_2O_4$ remains stable at 93.7% across 20 redox cycles. Although partial sintering and agglomeration was observed, the $Ca_2Fe_2O_5$ oxygen carrier has a fast reaction rate, high oxygen release and storage capacity, and excellent thermal stability over multiple redox cycles which makes the $Ca_2Fe_2O_5$ a promising candidate as an oxygen carrier for the TCLHG process with inherent CO_2 separation.

The carbon deposition characteristics of $Ca_2Fe_2O_5$ and $CaFe_2O_4$ samples was also explored to minimize carbon deposition during oxygen carrier reduction. The effect of reducing agent concentration and reduction temperatures on the carbon deposition was investigated to maximize reduction activity, and minimize the amount of deposited carbon. A CO concentration of 20% in N_2, and reduction temperatures of 850 °C or 900 °C were one of the best operational conditions for the TCLHG process. Although some mechanisms, such as calcium ferrites reduction, iron and calcium oxide combination, and Fe_3C formation need to be verified and investigated further, it is anticipated that $Ca_2Fe_2O_5$ will be a promising oxygen carrier and catalyst which can be used for chemical looping applications as well as other clean energy conversion and production processes such as biomass gasification and steam methane reforming.

Acknowledgements

This work was supported by the US National Science Foundation (1632899) and the National Natural Science Foundation of China (51576042). The authors also express thanks to the Fundamental Research Funds for the Central Universities, the Foundation of Graduate Creative Program of Jiangsu (KYLX16-0200), and the Scholarship Award granted to the first author by the Ministry of Education and China Scholarship Council.

Appendix A. Supplementary materials

Supplementary data associated with this article can be found, in the online version, at http://dx.doi.org/10.1016/j.apenergy.2017.11.005.

References

[1] Chen S, Wang D, Xue Z, Sun X, Xiang W. Calcium looping gasification for high-concentration hydrogen production with CO2 capture in a novel compact fluidized bed: simulation and operation requirements. Int J Hydrogen Energy 2011;36:4887–99.
[2] Thursfield A, Murugan A, Franca R, Metcalfe IS. Chemical looping and oxygen permeable ceramic membranes for hydrogen production–a review. Energy Environ Sci 2012;5:7421–59.
[3] Dou B, Song Y, Wang C, Chen H, Yang M, Xu Y. Hydrogen production by enhanced-sorption chemical looping steam reforming of glycerol in moving-bed reactors. Appl Energy 2014;130:342–9.
[4] Kathe MV, Empfield A, Na J, Blair E, Fan L-S. Hydrogen production from natural gas using an iron-based chemical looping technology: Thermodynamic simulations and process system analysis. Appl Energy 2016;165:183–201.
[5] Ma S, Chen S, Soomro A, Xiang W. Effects of supports on hydrogen production and carbon deposition of Fe-based oxygen carriers in chemical looping hydrogen

generation. Int J Hydrogen Energy 2017;42:11006–16.
[6] Murugan A, Thursfield A, Metcalfe I. A chemical looping process for hydrogen production using iron-containing perovskites. Energy Environ Sci 2011;4:4639–49.
[7] Liang H. Study on the effect of CeO2 on Fe2O3/LaNiO3 as the oxygen carrier applied in chemical-looping hydrogen generation. Int J Hydrogen Energy 2015;40:13338–43.
[8] Liu W, Ismail M, Dunstan MT, Hu W, Zhang Z, Fennell PS, et al. Inhibiting the interaction between FeO and Al2O3 during chemical looping production of hydrogen. RSC Adv 2015;5:1759–71.
[9] Li F, Luo S, Sun Z, Bao X, Fan L-S. Role of metal oxide support in redox reactions of iron oxide for chemical looping applications: experiments and density functional theory calculations. Energy Environ Sci 2011;4:3661–7.
[10] Song Q, Liu W, Bohn CD, Harper RN, Sivaniah E, Scott SA, et al. A high performance oxygen storage material for chemical looping processes with CO 2 capture. Energy Environ Sci 2013;6:288–98.
[11] Khan MN, Shamim T. Investigation of hydrogen generation in a three reactor chemical looping reforming process. Appl Energy 2016;162:1186–94.
[12] Zhang X, Jin H. Thermodynamic analysis of chemical-looping hydrogen generation. Appl Energy 2013;112:800–7.
[13] Cho WC, Seo MW, Kim SD, Kang K, Bae KK, Kim CH, et al. Continuous operation characteristics of chemical looping hydrogen production system. Appl Energy 2014;113:1667–74.
[14] Chiesa P, Lozza G, Malandrino A, Romano M, Piccolo V. Three-reactors chemical looping process for hydrogen production. Int J Hydrogen Energy 2008;33:2233–45.
[15] Bohn CD, Müller CR, Cleeton JP, Hayhurst AN, Davidson JF, Scott SA, et al. Production of very pure hydrogen with simultaneous capture of carbon dioxide using the redox reactions of iron oxides in packed beds. Ind Eng Chem Res 2008;47:7623–30.
[16] Cho P, Mattisson T, Lyngfelt A. Comparison of iron-, nickel-, copper-and manganese-based oxygen carriers for chemical-looping combustion. Fuel 2004;83:1215–25.
[17] Jin H, Ishida M. A new type of coal gas fueled chemical-looping combustion. Fuel 2004;83:2411–7.
[18] Lyngfelt A, Leckner B, Mattisson T. A fluidized-bed combustion process with inherent CO 2 separation; application of chemical-looping combustion. Chem Eng Sci 2001;56:3101–13.
[19] Mattisson T, Järdnäs A, Lyngfelt A. Reactivity of some metal oxides supported on alumina with alternating methane and oxygen application for chemical-looping combustion. Energy Fuels 2003;17:643–51.
[20] Wang S, Wang G, Jiang F, Luo M, Li H. Chemical looping combustion of coke oven gas by using Fe2O3/CuO with MgAl2O4 as oxygen carrier. Energy Environ Sci 2010;3:1353–60.
[21] Zafar Q, Mattisson T, Gevert B. Redox investigation of some oxides of transition-state metals Ni, Cu, Fe, and Mn supported on SiO2 and MgAl2O4. Energy Fuels 2006;20:34–44.
[22] Chen S, Shi Q, Xue Z, Sun X, Xiang W. Experimental investigation of chemical-looping hydrogen generation using Al2O3 or TiO2-supported iron oxides in a batch fluidized bed. Int J Hydrogen Energy 2011;36:8915–26.
[23] Gu Z, Li K, Qing S, Zhu X, Wei Y, Li Y, et al. Enhanced reducibility and redox stability of Fe2O3 in the presence of CeO2 nanoparticles. RSC Adv 2014;4:47191–9.
[24] Li F, Sun Z, Luo S, Fan L-S. Ionic diffusion in the oxidation of iron—effect of support and its implications to chemical looping applications. Energy Environ Sci 2011;4:876–80.
[25] Sarshar Z, Kleitz F, Kaliaguine S. Novel oxygen carriers for chemical looping combustion: La 1 − x Cex BO3 (B = Co, Mn) perovskites synthesized by reactive grinding and nanocasting. Energy Environ Sci 2011;4:4258–69.
[26] Boopathi KM, Mohan R, Huang T-Y, Budiawan W, Lin M-Y, Lee C-H, et al. Synergistic improvements in stability and performance of lead iodide perovskite solar cells incorporating salt additives. J Mater Chem A 2016;4:1591–7.
[27] Ismail M, Liu W, Scott SA. The performance of Fe 2 O 3-CaO oxygen carriers and the interaction of iron oxides with CaO during chemical looping combustion and H 2 production. Energy Procedia 2014;63:87–97.
[28] Hirabayashi D, Sakai Y, Yoshikawa T, Mochizuki K, Kojima Y, Suzuki K, et al. Mössbauer characterization of calcium-ferrite oxides prepared by calcining Fe 2 O 3 and CaO. ICAME 2005;2007:809–13.
[29] Zamboni I, Courson C, Kiennemann A. Fe-Ca interactions in Fe-based/CaO catalyst/sorbent for CO 2 sorption and hydrogen production from toluene steam reforming. Appl Catal B 2017;203:154–65.
[30] Ismail M, Liu W, Dunstan MT, Scott SA. Development and performance of iron based oxygen carriers containing calcium ferrites for chemical looping combustion and production of hydrogen. Int J Hydrogen Energy 2016;41:4073–84.
[31] Chan MS, Liu W, Ismail M, Yang Y, Scott SA, Dennis JS. Improving hydrogen yields, and hydrogen: steam ratio in the chemical looping production of hydrogen using Ca 2 Fe 2 O 5. Chem Eng J 2016;296:406–11.
[32] Kimura M, Uemura Y, Takayama T, Murao R, Asakura K, Nomura M. In situ QXAFS observation of the reduction of Fe2O3 and CaFe2O4. Journal of Physics: Conference Series: IOP Publishing; 2013. p. 012074.
[33] SIMMONS G, MUSIĆ S. Characterization of electric arc furnace dust by Mössbauer spectroscopy, Lehigh University, Bethlehem, Pennsylvania 1981, unpublished results. Google Scholar.
[34] Said AE-AA, El-Wahab MMA, Goda MN. Synthesis and characterization of pure and (Ce, Zr, Ag) doped mesoporous CuO-Fe 2 O 3 as highly efficient and stable nanocatalysts for CO oxidation at low temperature. Appl Surf Sci 2016;390:649–65.
[35] Deng Z, Xiao R, Jin B, Song Q, Huang H. Multiphase CFD modeling for a chemical looping combustion process (fuel reactor). Chem Eng Technol 2008;31:1754–66.
[36] Kwak BS, Park N-K, Baek J-I, Ryu H-J, Kang M. Effect of oxidation states of Mn in Ca1 − xLixMnO3 on chemical-looping combustion reactions. Korean J Chem Eng 2017;1–8.
[37] Liu W, Shen L, Gu H, Wu L. Chemical looping hydrogen generation using potassium-modified iron ore as an oxygen carrier. Energy Fuels 2016;30:1756–63.